

oml

**OAK RIDGE
NATIONAL
LABORATORY**

MARTIN MARIETTA



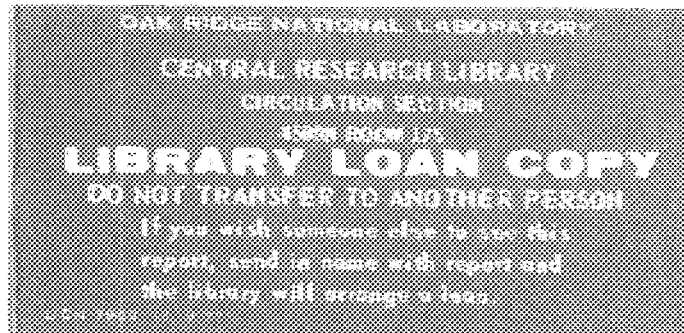
3 4456 0149069 3

ORNL/TM-10166

Metal Hydride Temperature Amplifiers for High Temperature (>260°C) Applications—A Parametric Study

Final Report

M. R. Ally



OPERATED BY
MARTIN MARIETTA ENERGY SYSTEMS, INC.
FOR THE UNITED STATES
DEPARTMENT OF ENERGY

Printed in the United States of America. Available from
National Technical Information Service
U.S. Department of Commerce
5285 Port Royal Road, Springfield, Virginia 22161
NTIS price codes--Printed Copy: A04 Microfiche A01

This report was prepared as an account of work sponsored by an agency of the United States Government. Neither the United States Government nor any agency thereof, nor any of their employees, makes any warranty, express or implied, or assumes any legal liability or responsibility for the accuracy, completeness, or usefulness of any information, apparatus, product, or process disclosed, or represents that its use would not infringe privately owned rights. Reference herein to any specific commercial product, process, or service by trade name, trademark, manufacturer, or otherwise, does not necessarily constitute or imply its endorsement, recommendation, or favoring by the United States Government or any agency thereof. The views and opinions of authors expressed herein do not necessarily state or reflect those of the United States Government or any agency thereof.

ENERGY DIVISION

METAL HYDRIDE TEMPERATURE AMPLIFIERS FOR
HIGH TEMPERATURE (>260°C) APPLICATIONS--
A PARAMETRIC STUDY

FINAL REPORT

Moonis R. Ally

Date Published-December 1986

Prepared by the
Oak Ridge National Laboratory
Oak Ridge, Tennessee 37831
Operated by
MARTIN MARIETTA ENERGY SYSTEMS, INC.
for the
Office of Industrial Programs
U.S. DEPARTMENT OF ENERGY
under Contract No. DE-AC05-84OR21400



3 4456 0149069 3

PREFACE

This document was prepared for the U.S. Department of Energy (DOE) Office of Industrial Programs (OIP) as part of the OIP Chemical Heat Pump Study. The development of the computer program and analysis was performed at the Oak Ridge National Laboratory, whereas the data collection on hydriding alloys was available from a recent DOE study (contract number DE-AC07-84ID12520).

Particular thanks are due Mr. R. N. Chappell of DOE Idaho Operations Office; Mr. Scott Richlen of DOE/OIP, Washington, D. C.; and Mr. Stephen Kaplan of ORNL for their support in probing hydride technology.

CONTENTS

	<u>Page</u>
LIST OF FIGURES	vii
NOMENCLATURE	ix
EXECUTIVE SUMMARY	xi
ABSTRACT	1
1. INTRODUCTION	2
1.1 Background	2
1.2 Absorption Isotherms	3
1.3 Van't Hoff Curves	3
2. APPLICATION OF HYDRIDES IN TEMPERATURE AMPLIFIERS	9
3. ACHIEVING PRESCRIBED DELIVERY TEMPERATURES WITH METAL HYDRIDES	11
4. COMPUTER PROGRAM DEVELOPMENT	16
5. RESULTS AND ANALYSIS	17
6. ABSORPTION BED DESIGN PARAMETERS	21
6.1 The Mass Transfer Zone (MTZ) Concept	21
6.2 Design Equations	21
6.2.1 Mass Transfer	21
6.2.2 Heat Transfer	23
7. CYCLIC STABILITY, DECREPITATION, KINETICS AND COSTS	26
7.1 Stability	26
7.2 Decrepitation	26
7.3 Reaction Kinetics	26
7.4 Costs and Availability	27
REFERENCES	28
APPENDIX	29

LIST OF FIGURES

<u>Figure</u>	<u>Page</u>
1. Ideal pressure-composition (P-C) isotherm for a metal hydride	4
2. Dynamic P-C isotherms for LaNi_5 . One set of isotherms is shown for comparison which was determined by the "static" test procedure	5
3. Van't Hoff plots for alloys which show potential for high delivery temperatures in chemical heat pumps	6
4. TA cycle	10
5. Low cycle pressure and low temperature lift limitations using ZrCo (hot side) and ZrNi (cold side) alloys in a three-temperature TA cycle	12
6. Three-temperature TA cycle using Mg_2Ni (hot side) and $\text{Ti}_{0.95}\text{V}_{0.05}\text{Co}$ (cold side) alloys to attain 256°C (492°F) with waste heat source at 163°C (325°F)	13
7. Four-temperature TA cycles showing how they may achieve high delivery temperature within reasonable pressure limits	14
8. Hot and cold side alloy inventories per bed as a function of H/M ratios and cycle times for a three-temperature TA ($T_H = 253.8^\circ\text{C}$, $T_M = 162.2^\circ\text{C}$, $T_L = 105.6^\circ\text{C}$)	18
9. Hot and cold side alloy inventories per bed as a function of H/M ratios and cycle times for a four-temperature TA ($T_H = 301.1^\circ\text{C}$, $T_M' = 166.1^\circ\text{C}$, $T_L = 132.2^\circ\text{C}$)	19
10. Mass transfer zone (MTZ) and adsorbate loading curves during various stages of absorption	22

NOMENCLATURE

A	absorbent bed cross-sectional area, m^2
D	diameter, m
G_s	superficial mass velocity of feed stream, $kg/m^2 \cdot min$
ΔH	heat of absorption, kJ/mole
h_a	heat transfer coefficient, $W/m^2 \cdot K$
k_a	thermal conductivity of adsorbent, $W/m \cdot K$
k_t	thermal conductivity of tube materials, $W/m \cdot K$
L	bed length, m
V	heat transfer rate per unit volume, $kJ/min \cdot m^3$
Q	heat transfer rate, $kJ/m^2 \cdot min$
R	radius of inner tube containing adsorbent, m
R_1	radius of outer tube containing adsorbent, m
T_1, T_0	temperatures, K
w	mass of hydrogen absorbed, kg
x	adsorbent loading in bed, $kg H_2/kg$ alloy
ρ_b	density of packed adsorbent bed, kg/m^3
$\Delta \theta$	time interval, min

EXECUTIVE SUMMARY

This document is aimed at judging whether present-day hydriding alloys can viably serve as working media for high-temperature ($\geq 260^\circ\text{C}$) heat pump devices.

Extensive pertinent literature on hydrides was available from a recent (1985, unpublished) DOE study. In spite of copious information, only three hydrides (ZrCo, ZrNi and Mg_2Ni) were found capable of reaching temperatures $\geq 260^\circ\text{C}$ within an operating pressure range of 10 to 0.1 atm. The moderate pressures help keep equipment fabrication costs low.

It was discovered that the conventional temperature amplifier (TA) cycle operating on a three-temperature basis could barely be used in any meaningful way to achieve 260°C delivery temperature. In order to circumvent this obstacle, a newly proposed four-temperature TA cycle is discussed whose use, it is believed, will be mandatory with present-day hydriding alloys.

The U.S. industrial constituency demands at least a two-year pay-back on its investments. With present energy costs at $\$4.74/10^6$ kJ ($\$/10^6$ Btu), an 8.79×10^6 W (30×10^6 Btu/h) TA would save the equivalent of $\$2.4 \times 10^6$ in two years. If installation costs are 100% of capital costs and if equipment and material (alloy) costs are of equal magnitude, then alloy costs work out to be $\$6 \times 10^5$. In continuous operation, a battery of at least four adsorption beds will be needed, bringing the alloy costs per bed to $\$1.5 \times 10^5$. Presently, the estimated minimum cost of alloy production is $\$33.07/\text{kg}$ which limits the quantity of alloy in each adsorption bed to about 4535 kg.

The computed results show that under the most optimistic conditions of favorable hydrogen to metal (H/M) ratios, cycle times, alloy durability, and cycling stability, at least 15,900-22,700 kg of alloy per bed would be required, with the present state of hydride technology. Lower alloy inventories would be possible by decreasing cycle time from 20 min to about 5 min, but it is shown that this is practically impossible within temperature and design constraints.

In addition to cycle times, a further liability of hydrides is that their durability has never been tested over long periods (>2 years) under continuous cycling (charging/discharging) conditions. One reason is that most hydrides break down in size after about 300 cycles. The breakdown is not detrimental other than causing an increased pressure drop and plugging problems. However, it has been observed that reduction in H/M ratio caused by disproportionation and traces of impurity (CO , CO_2 , O_2 , etc.) are plaguing problems which usually limit alloy life from six months to even a matter of days. Under these circumstances, metal hydrides do not appear to be viable for heat pump applications.

An interactive FORTRAN computer program developed during this work enables the user to calculate alloy requirements for a given set of input information.

METAL HYDRIDE TEMPERATURE AMPLIFIERS FOR
HIGH-TEMPERATURE (>260°C) APPLICATIONS--
A PARAMETRIC STUDY

Moonis R. Ally

ABSTRACT

The viability of hydriding alloys as working media in heat pumps to achieve temperature boosts up to 260°C or better, is investigated on the basis of the mass transfer zone concept of absorption bed design and a return on capital investment of two years.

The Van't Hoff curves for various metals in the temperature and pressure ranges of interest were found in the open literature. An integrated form of the Clausius-Clapeyron equation was used to describe the equilibrium hydrogen pressure-temperature relationship. Design equations pertaining to overall material and heat balances are presented. An inherent assumption in the development of these equations is that of steady state operation. Other, more stringent assumptions pertain to cycling stability, resistance to poisoning, constant absorption capacity and durability of the metal over a two year period. The design equations along with the necessary thermodynamic data are incorporated in an interactive FORTRAN computer program called HYDRIDE which determines the quantity of metal required per bed for an 8.79×10^6 W (30×10^6 Btu/h) temperature amplifier.

The computer results show that even under the optimistic assumptions of the model, the estimated metal required per bed would be between 15,900 and 22,700 kg, depending on the particular metals chosen. Based on a metal cost of \$33.07/kg and cost of energy at \$5/10⁶ Btu, the maximum permissible metal in each bed for a two year payback works out to be 4535 kg. It is therefore concluded that even under very optimistic conditions, hydriding alloys are economically unattractive for heat pump applications.

1. INTRODUCTION

1.1 Background

Some metals have the unusual property of reacting with hydrogen at room temperature and near atmospheric pressure when brought into physical contact with it. Such metals include elements like palladium, magnesium, and alloys, commonly referred to as hydriding metals.

During physical contact, hydrogen molecules are first adsorbed onto the surface of the metal. Some of the molecules dissociate into hydrogen atoms (H), which subsequently enter the crystal lattice of the metal to occupy specific sites among the metal atoms. Such locations are called interstitial sites. They must possess a certain minimum volume in order to easily accommodate the hydrogen atom. As the pressure of the hydrogen gas above a hydriding metal is increased (by external means), a limited number of atoms are forced into the crystal. Usually at some critical concentration and pressure the metal becomes saturated with hydrogen and goes into a new phase called the metal-hydride phase. If the hydrogen pressure is only slightly increased, much greater amounts of hydrogen are absorbed. Ultimately, all the original hydrogen saturated metal phase will be converted into the metal-hydride phase. Since metal crystals have many interstitial sites, it is possible for them to accommodate large amounts of hydrogen in a highly compact manner. In many hydrides, the number of hydrogen atoms in the crystal will be two or three times the number of metal atoms. Hydrogen within the metal crystal can be released by warming the metal alloy. The process of hydrogen absorption and desorption is therefore reversible and is generally represented by the following chemical reaction:



A specific example^{1,2} of Eq. 1 is the reaction of lanthanum pentanickel (one of the earliest compounds to be studied) with hydrogen.



The hydrogen capacity represented by the hydride is usually specified as the hydrogen to metal ratio (H/M) which in the above example is 1.0. This represents a weight capacity of about 1.4%. Volumetrically, the storage capacity of the alloy is a very impressive 1.1 liter H₂ (STP) per cc of alloy or about 80% more than that of pure liquid hydrogen. The large numerical disparity between the weight and volumetric capacities is due to the large density of the alloy.^{3,4} For further details, the reader is referred to the literature.

1.2 Absorption Isotherms

Absorption and desorption properties of hydriding metals are empirically determined from pressure-composition (P-C) diagrams. Starting with the metal phase at point 1 (Fig. 1), the pressure of the H_2 gas is slowly increased while the total system is maintained at constant temperature. A small quantity of hydrogen permeates into the alloy until point 2 is reached when the hydriding reaction commences with relatively large quantities of hydrogen being absorbed at nearly constant pressure. The nearly constant pressure part of the P-C curve corresponds to a two-phase mixture of metal, Me, and metal hydride, MeH_x in equilibrium with the gaseous H_2 phase. At point 3, the alloy has been completely converted to the hydride phase and a further increase in applied H_2 pressure up to point 4 results in a nominal pickup of hydrogen in solution in the hydride phase. In principle the P-C curve is reversible. As the total pressure above the alloy is lowered, the metal hydride phase dissociates to $Me + H_2$ liberating H_2 as it traces the reverse path, 4-3-2-1. In practice, the plateau pressure is never completely flat and the reverse (dehydriding) curve is never retraced with fidelity, especially with regard to the flat plateau. The discrepancy between the hydriding and dehydriding curves is known as hysteresis and depends upon other factors such as the way in which the process was conducted (static vs dynamic). The hysteresis effect for $LaNi_5$ is shown in Fig. 2 (ref. 2).

1.3 Van't Hoff Curves

An examination of Fig. 2 shows that the plateau pressure increases with temperature. This trend is common to all metal hydrides. The plateau pressure dependence on temperature for a given alloy is represented by plotting pressure on the ordinate and the corresponding temperature or its reciprocal on the abscissa, in accordance with the Van't Hoff equation given by:

$$2.3 \log P = \ln P = \frac{\Delta H}{RT} - \frac{\Delta S}{R}, \quad (3)$$

where ΔH and ΔS are the enthalpy and entropy changes respectively of the hydriding reaction. The magnitude of ΔH varies widely with different alloys. For reactions of the type represented by Eq. 1, the hydriding reaction (\rightarrow) is exothermic and the dehydriding reaction (\leftarrow) is endothermic. The difference in entropy of hydrogen between its gaseous and metal hydride states is ΔS and varies only slightly from alloy to alloy.

The values of ΔH and ΔS can easily be obtained from experimental isotherms by plotting plateau pressure vs the reciprocal absolute temperature as shown in Fig. 3. Such plots are commonly known as Van't Hoff plots. Most data fall on a straight line over moderate temperature limits. If Eq. 3 is applied to the Van't Hoff plots, the slope

ORNL-DWG 86-7980

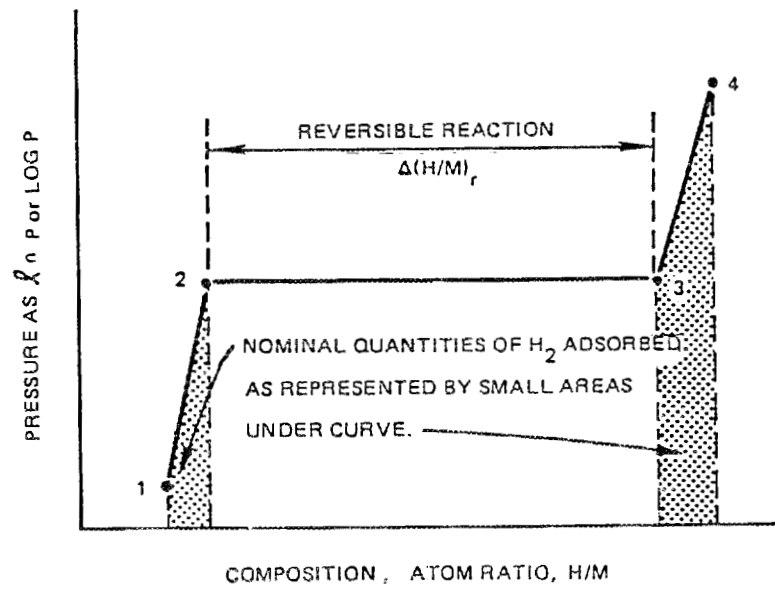


Fig. 1. Ideal pressure-composition (P-C) isotherm for a metal hydride.

ORNL-DWG 86-7982

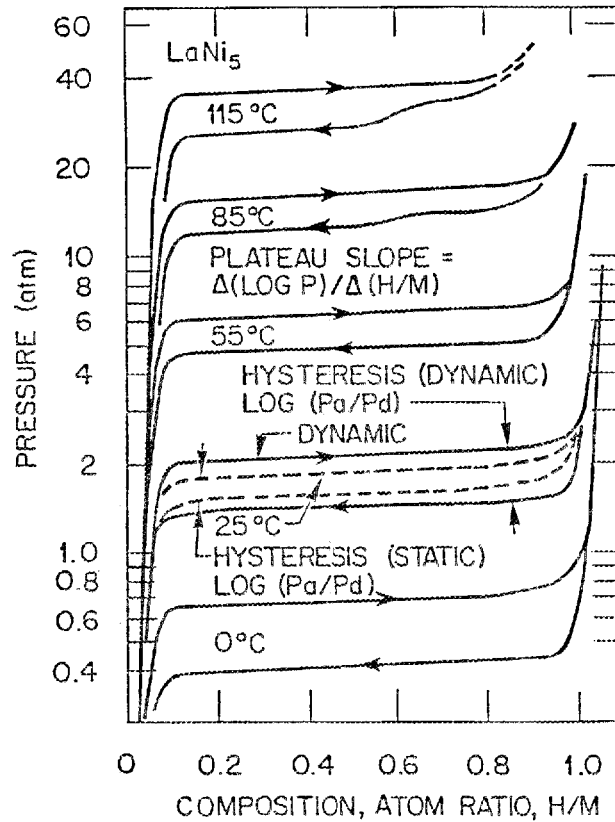


Fig. 2. Dynamic P-C isotherms for LaNi₅. One set of isotherms is shown for comparison which was determined by the "static" test procedure. [1 atm = 1.013×10^5 Pa]

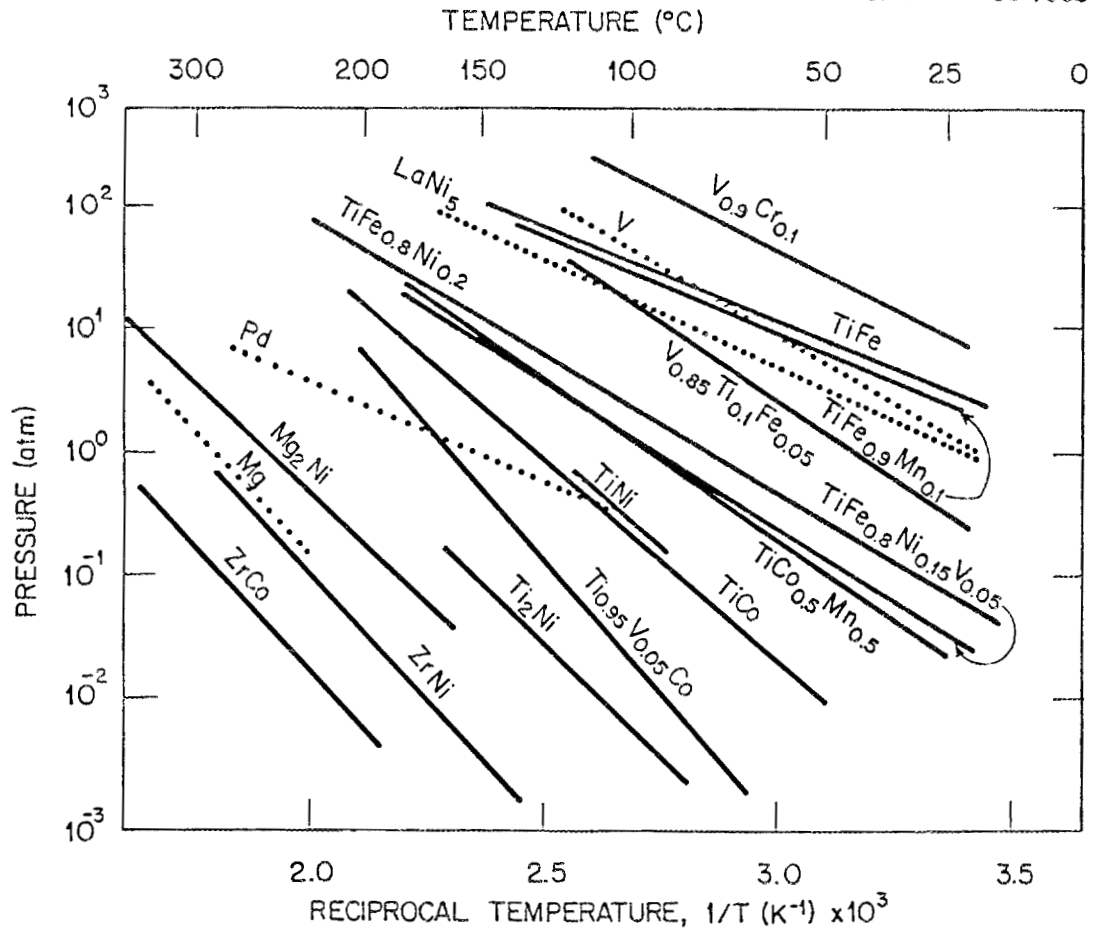


Fig. 3. Van't Hoff plots for alloys which show potential for high delivery temperatures in chemical heat pumps. [1 atm = 1.013×10^5 Pa]

represents ΔH and the intercept on the ordinate when $1/T = 0$ (infinite temperature) represents ΔS .

A more convenient way to represent the data in Fig. 3 is by utilizing the equation,

$$2.3 \log P = \ln P = \frac{A}{T} + B, \quad (4)$$

which can also be put in the differential form,

$$\frac{d \ln P}{d\left(\frac{1}{T}\right)} = A. \quad (5)$$

Equation 5 bears a very close resemblance to the Clausius-Clapeyron equation,

$$\frac{d \ln P}{d\left(\frac{1}{T}\right)} = \frac{\Delta H}{R}, \quad (6)$$

which represents an equation for the phase change of a pure substance. In fact, the absorption of hydrogen and formation of the hydride phase is a phase change from gaseous H_2 to a state in a solid solution. Since the forces binding H_2 in the metal interstices are stronger than the attractive forces between adjacent molecules in the liquid state but weaker than chemical bond forces, the magnitude of ΔH lies somewhere in between those of heats of vaporization and chemical reaction. Equations 5 and 6 also indicate that ΔH can be evaluated from a knowledge of the empirical constant, A.

The pressure and reciprocal temperature relationships of nine selected alloys from Fig. 3 were correlated by the equation, $\log P = A/T + B$. The equations, temperature range of validity, and ΔH values are summarized in Table 1.

Table 1. Summary of equations of the type, $\log P = A/T + B$,
for various alloys shown in Fig. 3

(P is in atmospheres)^a

Alloy	Integrated form of Clasius-Clapeyron type of equation	Temperature range of validity, K	Mass per atom of metal
ZrCo	$\log P = -4137/T + 6.486$	$465 < T < 625$	75.0
ZrNi	$\log P = -4025/T + 7.075$	$416 < T < 625$	74.95
Mg ₂ Ni	$\log P = -3534/T + 6.730$	$434 < T < 625$	35.78
Ti ₂ Ni	$\log P = -3578/T + 7.434$	$357 < T < 434$	51.50
Ti _{0.95} V _{0.05} Co	$\log P = -4221/T + 9.733$	$344 < T < 476$	53.50
TiCo	$\log P = -3204/T + 7.993$	$322 < T < 476$	53.42
TiCo _{0.5} Mn _{0.5}	$\log P = -2412/T + 6.604$	$294 < T < 454$	52.42
TiFe _{0.8} Ni _{0.15} V _{0.05}	$\log P = -2297/T + 6.358$	$294 < T < 454$	51.97
TiFe _{0.8} Ni _{0.2}	$\log P = -2199/T + 6.324$	$285 < T < 500$	52.16

^a1 atm = 1.013×10^5 Pa.

2. APPLICATION OF HYDRIDES IN TEMPERATURE AMPLIFIERS

In the temperature amplifier (TA) configuration, a hydride heat pump uses waste heat at an intermediate temperature, T_M , to achieve a higher temperature, T_H . Of course, in cyclic operations in order to maintain thermodynamic consistency, heat must be rejected at a temperature T_L , lower than T_M . The TA configuration is shown in Fig. 4. Referring to this figure, one notes that the TA consists of two alloys which, for historical reasons, are classified as the hot and cold side alloys. The rationale for this classification stems from the fact that at a given hydrogen pressure, the hot side alloy is the one whose corresponding equilibrium temperature is the highest. The hot side alloy is sometimes also referred to as the low pressure alloy because at a given temperature its equilibrium pressure is lower than the cold side alloy, the latter now being called the high pressure alloy.

As shown in Fig. 4, heat from a waste source at T_M desorbs hydrogen from the hot side alloy at point 1. The desorbed hydrogen is absorbed onto the cold side alloy at 2, with the enthalpy of absorption rejected to the surroundings at T_L . The hydrogen pressure in the cold side alloy is increased to its equilibrium value at T_M by supplying heat from the waste stream (point 3). The hydrogen is then desorbed at 3 and absorbed at 4, with the heat of absorption released at the equilibrium temperature, T_H . Unlike the idealization shown in Fig. 4, in actual practice a certain pressure drop must exist in transporting hydrogen between the vessels containing the hot and cold side alloys at the prescribed mass flow rate. These pressure drops contribute to parasitic losses, lowering the overall cycle efficiency.^{1,5}

Other important design considerations related to the application of metal hydrides to heat amplifiers or the refrigeration cycles can be found in the literature.^{1,2,4,6}

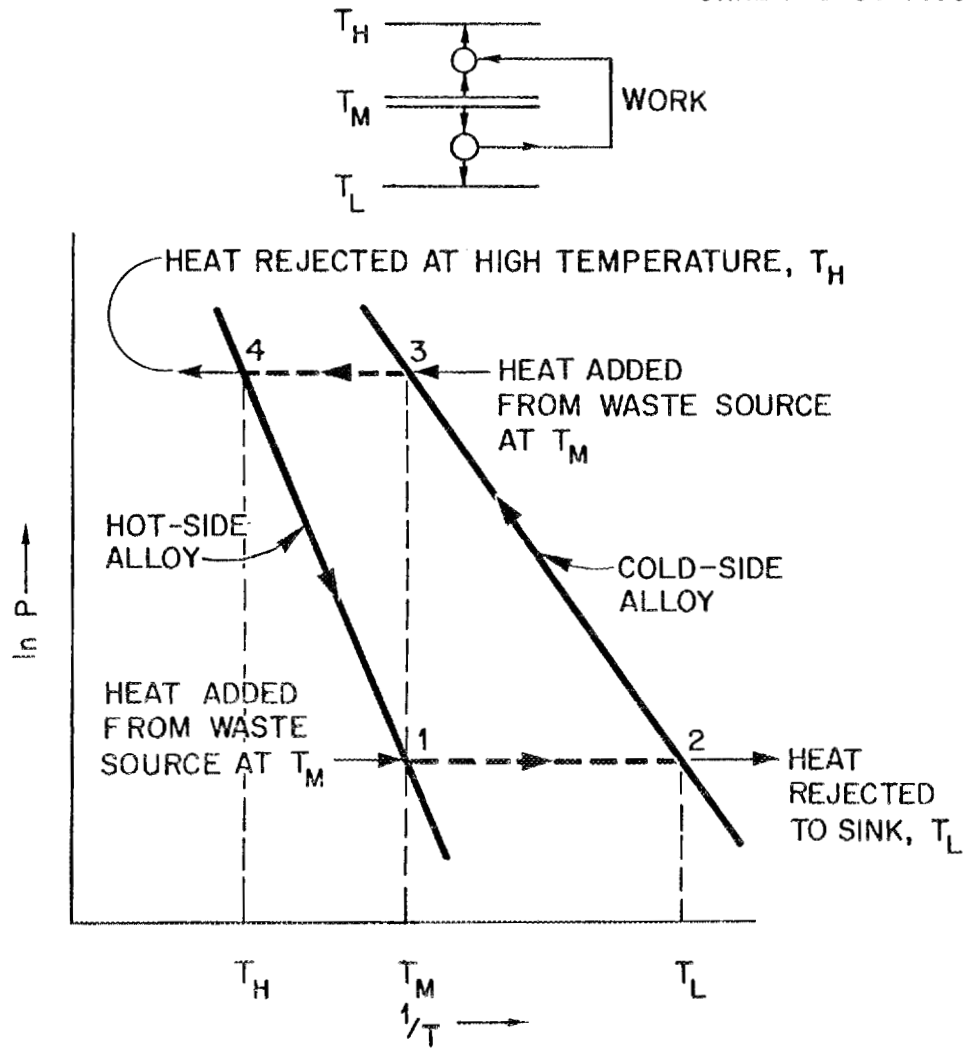


Fig. 4. TA cycle.

3. ACHIEVING PRESCRIBED DELIVERY TEMPERATURES WITH METAL HYDRIDES

One of the objectives of the Chemical Heat Pump program is to achieve delivery temperatures of at least 260°C (500°F) with high temperature lifts and reasonable pressures within the TA machine. The alloy Van't Hoff plots in Fig. 3 show that ZrCo, ZrNi and Mg₂Ni operate well beyond 260°C and therefore present themselves as strong candidates for hot side alloy selection. However, the constraint of reasonable operating pressures levies a restriction on ZrCo and ZrNi in terms of finding suitable cold side partners. This is especially so if the TA in question operates on the three-temperature basis of Fig. 4. An example will clarify this point. Suppose ZrCo is selected as the hot side alloy. At 260°C, the equilibrium hydrogen pressure is 5369 Pa (0.053 atm). With a three-temperature cycle, the solitary cold side alloy for ZrCo is ZrNi. Figure 5 shows that the waste heat source temperature must be 208°C (407.6°F) and the pressure, an impractical value of 777.6 Pa (0.0077 atm). It should be clear from the data of Fig. 3 that there is virtually no other cold side alloy that can be used in combination with ZrCo or ZrNi which will satisfy DOE's pressure (10^6 to 3×10^3 Pa) and temperature boost ($\geq 260^\circ\text{C}$) criteria. It will be shown later how this difficulty may be circumvented by resorting to a four-temperature TA cycle, but first the discussion on the three-temperature cycle needs to be completed. Further pondering shows that in a three-temperature TA cycle, only two of the alloys of Fig. 3, viz., Mg₂Ni (hot side) and Ti_{0.95}V_{0.05}Co (cold side), will meet DOE's temperature and pressure criteria. This cycle is depicted in Fig. 6.

Returning to ZrCo and ZrNi alloys, it will be demonstrated how they can be used in combination with other alloys in Fig. 3 to attain 500°F delivery temperature or better, and yet be within the limits of reasonable pressures. Such an achievement is possible by considering a four-temperature TA cycle. Examples will best illustrate this point. Consider the scenario in Fig. 7(a) with ZrCo as the hot side alloy. Suppose waste heat is available at 253°C (487°F). The equilibrium hydrogen pressure for ZrCo at this temperature is 4279 Pa (0.0422 atm) as indicated by point 1. If Ti₂Ni is chosen as the cold side alloy, the sink temperature must be 133.2°C (271°F) (point 2). If hydrogen is now desorbed from Ti₂Ni with a waste stream at 167°C (331°F) (point 3) and absorbed by ZrCo, the resulting delivery temperature will be 302°C (576°F) (point 4). The lowest and highest pressures in the cycle, 4265 Pa and 2.0×10^4 Pa (32 mm Hg and 152 mm Hg), are within reasonable limits for CHPs. In this case the temperature lift is not clearly defined because of the involvement of two intermediate waste heat temperatures, but it is at least equal to 49.5°C (302.2°C - 252.7°C). High delivery temperatures may be attained with ZrCo and Ti_{0.95}V_{0.05}Co [Fig. 7(b)], ZrNi and TiCo [Fig. 7(c)], or with Mg₂Ni and TiCo [Fig. 7(d)]. The flexibility and high delivery temperatures offered by a four-temperature

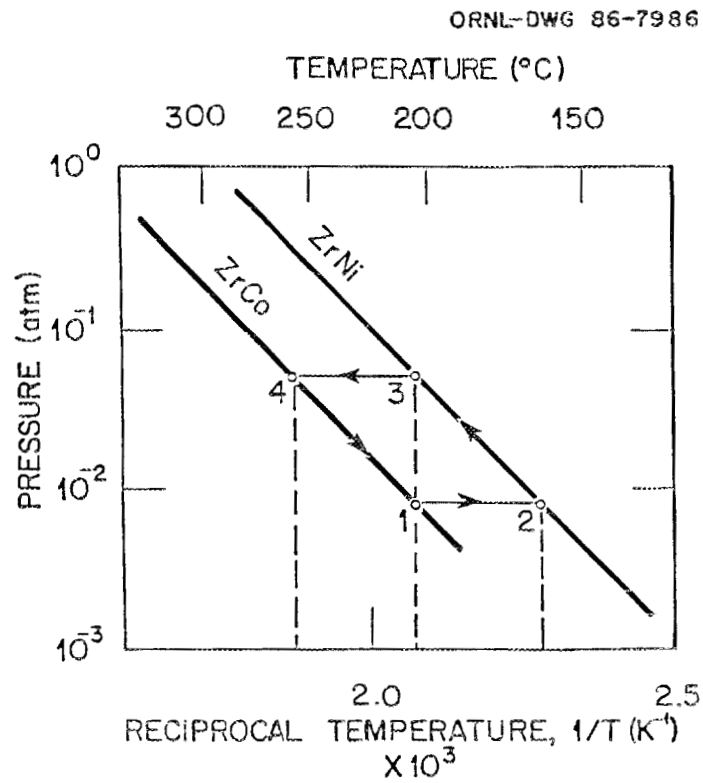


Fig. 5. Low cycle pressure and low temperature lift limitations using ZrCo (hot side) and ZrNi (cold side) alloys in a three-temperature TA cycle. [1 atm = 1.013×10^5 Pa]

ORNL-DWG 86-7984

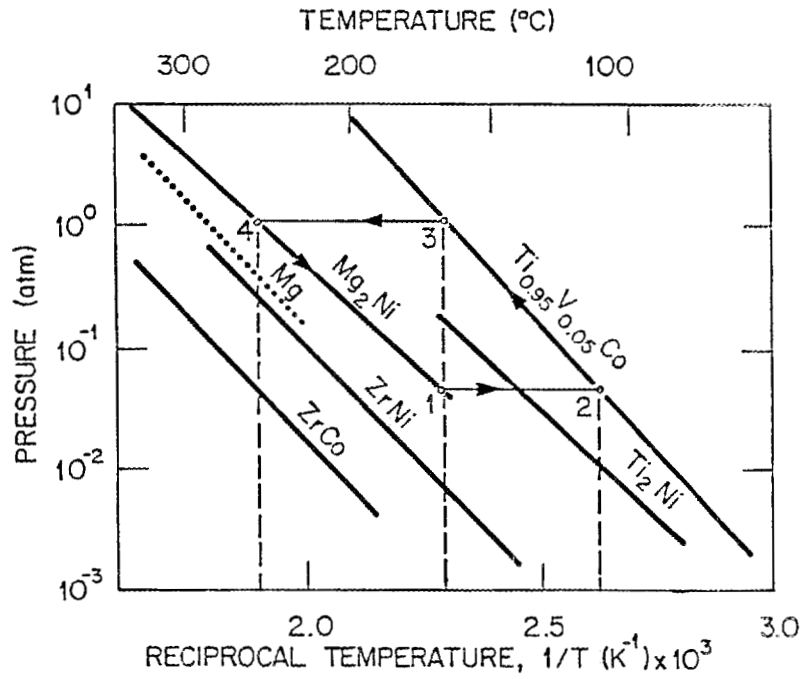
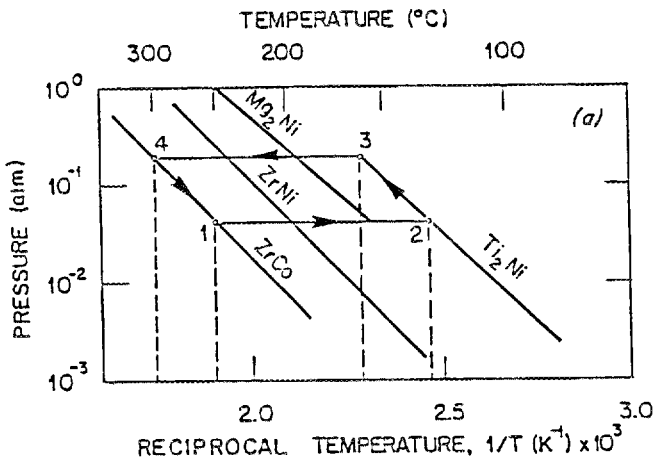
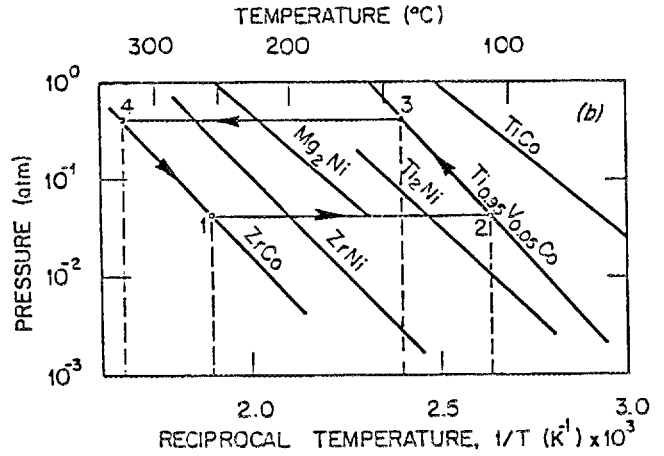


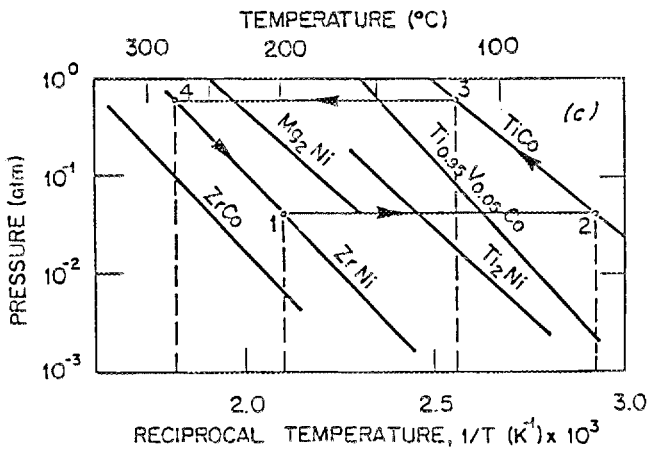
Fig. 6. Three-temperature TA cycle using Mg₂Ni (hot side) and Ti_{0.95}V_{0.05}Co (cold side) alloys to attain 256°C (492°F) with waste heat source at 163°C (325°F). [1 atm = 1.013×10^5 Pa]



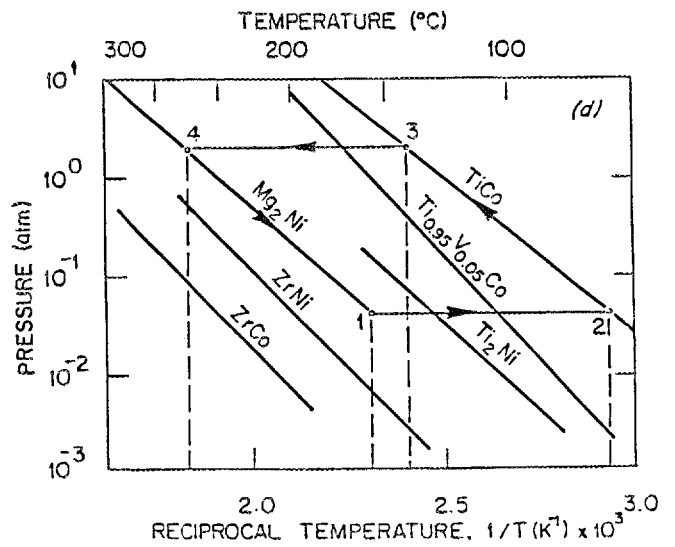
(a) ZrCo (hot side) and Ti_2Ni (cold side)



(b) ZrCo (hot side) and $Ti_{0.95}V_{0.05}Co$ (cold side)



(c) ZrNi (hot side) and TiCo (cold side)



(d) Mg_2Ni (hot side) and TiCo (cold side)

Fig. 7. Four-temperature TA cycles showing how they may achieve high delivery temperature within reasonable pressure limits. [1 atm = 1.013×10^5 Pa]

cycle opens the possibility of various hydride combinations. Such flexibility was impossible using a three-temperature TA cycle.

4. COMPUTER PROGRAM DEVELOPMENT

An interactive FORTRAN program was written to evaluate the TA cycle for any paired combination of alloys. The input data consists of identifying the hot and cold side alloys by specific numbers (shown in a menu), the waste heat source temperature(s) ($^{\circ}\text{F}$), desired heat pump capacity (Btu/h), the H/M ratios for the two alloys, and the cycle time (min) of each absorbent bed. More will be said about the cycle time later. The computer output consists of a systematic listing of the input data and the calculated values of the delivery temperature, quantities of required hot and cold side alloys (lb), the pressure values (atm), and the coefficient of performance (COP, dimensionless).

Listing of the FORTRAN program called HYDRIDE and examples of outputs are in the Appendix.

5. RESULTS AND ANALYSIS

It has been shown [Figs. 7(a)-7(d)] that in principle, it is possible to use hydrides in certain ways to attain delivery temperatures even greater than 500°F (260°C) within the constraints of moderate pressures (10-0.03 atm). However, the bridge between proof of principle and practical application is a wide one encompassing issues of hardware configuration and economic necessities. Towards the goal of evaluating the hydrides objectively, both the practical and economic aspects will be considered but the tipping of the scales either in the direction of favor or disfavor will be done by economic considerations. This is because in the industrial heat pump constituency, there is a tacit understanding that even a perfect heat pump must have less than a two-year payback period.

For the purpose of analysis, a baseline case of a 30×10^6 Btu/h (8.79×10^6 W) TA is considered. The selection of this capacity is another legacy inherited from an earlier era of mechanical heat pumps. The present value of energy is taken as $\$5/10^6$ Btu. If industry adheres to the two-year payback limitation, the total energy produced by a TA within that period would be 30×10^6 Btu/h \times 8000 h/yr \times 2 yr = 4.80×10^{11} Btu valued at $\$4.80 \times 10^{11} \times 5.00/10^6 = \2.40×10^6 . Therefore the cost of equipment, installation, and operation during the two-year period must be no greater than $\$2.40 \times 10^6$.

If installation costs are 100% of capital costs, the cost of hydride material and equipment must be $\$1.20 \times 10^6$. Further, assuming material and equipment costs to be of equal proportion, the hydride costs become $\$0.6 \times 10^6$. For continuous operation, a minimum of four beds is required. Hence the material costs per bed work out as $\$1.5 \times 10^5$. At an estimated selling cost of $\$15/\text{lb}$ of alloy, the hydride requirements become 4535 kg/bed, if the material shows durability without loss of performance for two years.

The quantity of hydride material required for an 8.79×10^6 W TA machine under the assumptions discussed above is 4535 kg/bed in a battery of four beds.

The results of the computer program shown in Figs. 8 and 9 can be used to determine the conditions under which hydriding alloys may be economical for CHP applications.

An examination of Fig. 8 reveals that the hot side alloy inventory per bed varies linearly with cycle time for a constant value of the H/M ratio. This linear relationship is steep for low H/M and moderate for high H/M ratios, as may be expected. The range of H/M ratios for alloys varies between 0.2 and 1.0. However, the alloys with values near unity are typically low-temperature AB₅ type alloys like LaNi₅. The AB₅ type alloys would be unsuitable for attaining high temperatures because the pressures would be prohibitively high. Therefore, the H/M ratios in Fig. 8 were varied from 0.2 to 0.7 and this range is considered to be representative of high temperature alloys. At high cycle times (40-45 min), the mass of alloy required remains very high even at H/M = 0.7

ORNL-DWG 86-7985

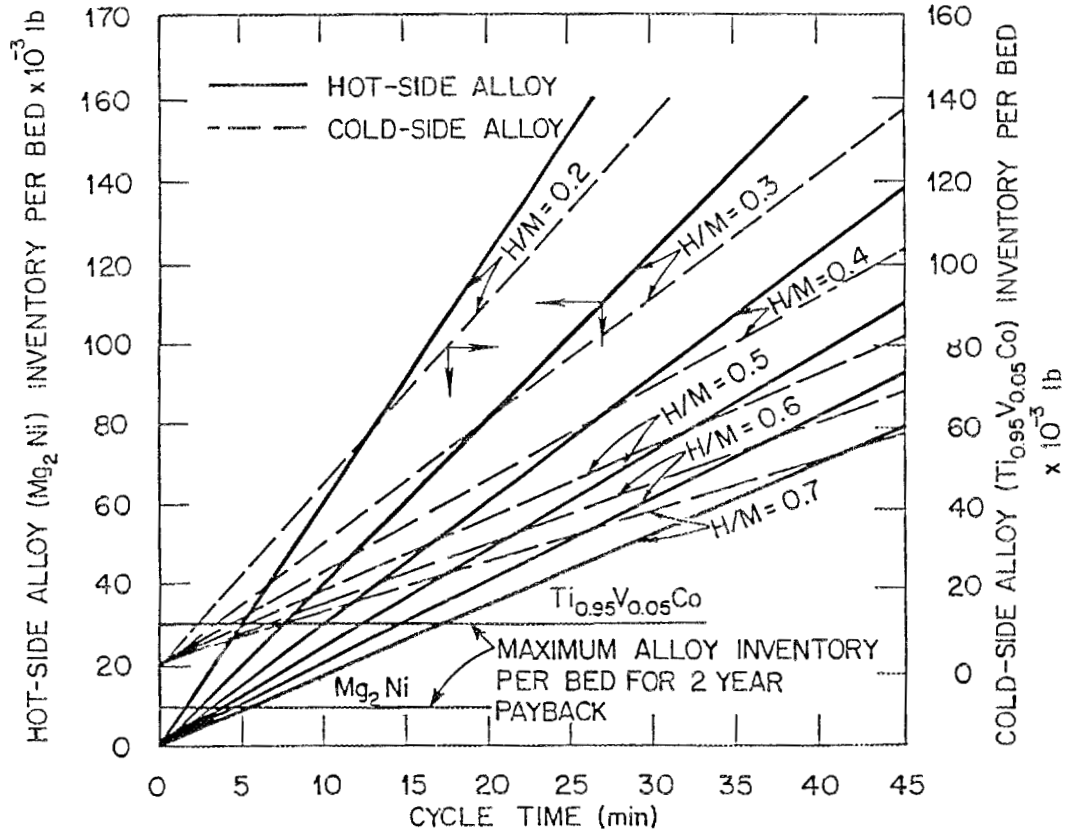


Fig. 8. Hot and cold side alloy inventories per bed as a function of H/M ratios and cycle times for a three-temperature TA ($T_H = 253.8^\circ C$, $T_M = 162.2^\circ C$, $T_L = 105.6^\circ C$). [1 lb = 0.4536 kg]

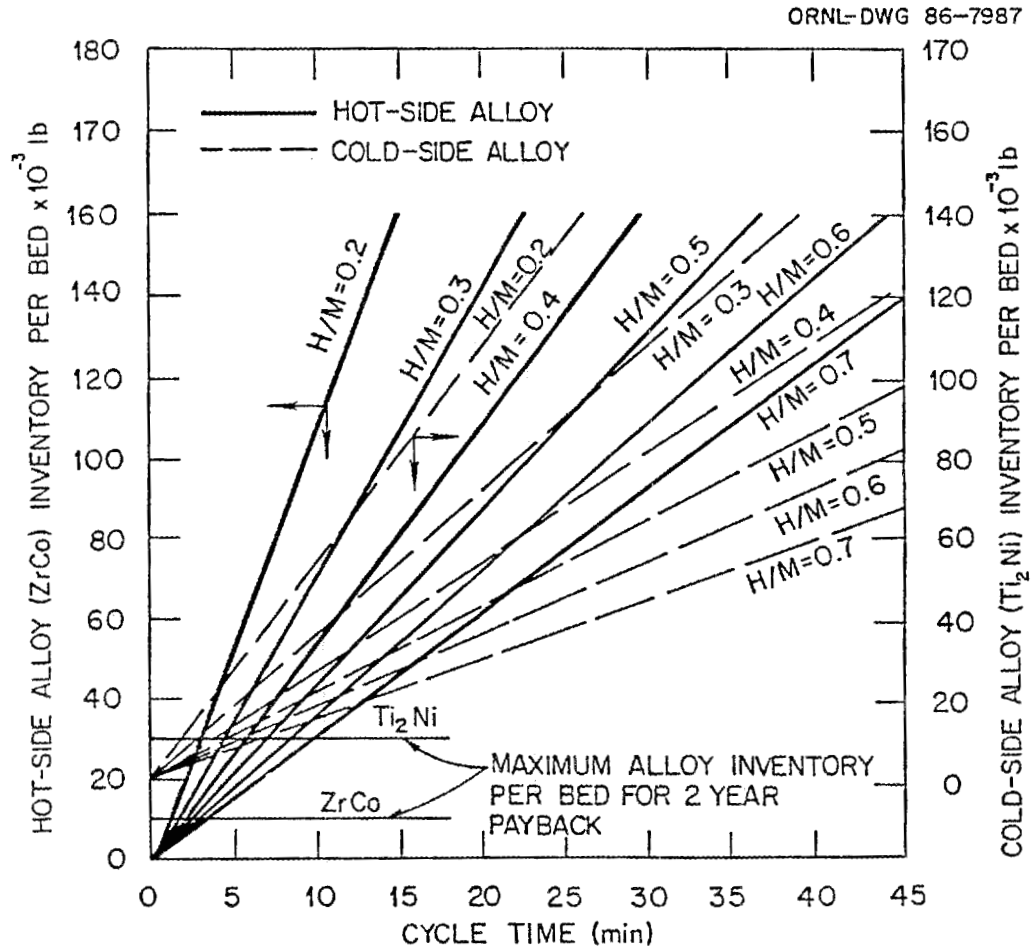


Fig. 9. Hot and cold side alloy inventories per bed as a function of H/M ratios and cycle times for a four-temperature TA ($T_H = 301.1^\circ C$, $T_M' = 166.1^\circ C$, $T_L = 132.2^\circ C$). [1 lb = 0.4536 kg]

(32,650-36,280 kg). At lower cycle times (5 min), the absolute mass of alloys is small (<13,600 kg) for any range of H/M values even though the proportional variation of alloy quantity with H/M remains the same at low and high cycle times. Since alloy quantity is directly related to material costs, the main conclusion of Fig. 8 is that metal hydride absorption beds must operate at low cycle times. To find out how low these cycle times have to be in order to satisfy the two-year payback period criterion, a straight line representing a constant alloy inventory of 4535 kg/bed is drawn as shown in Fig. 8. From its intersection with the parametric curves, it is obvious that under the most optimistic H/M value of 0.7 the maximum allowable cycle time is 5.5 min.

Figure 9 is the result for ZrCo (hot side) and Ti_2Ni (cold side) alloy in a four-temperature TA cycle. The only qualitative difference between the three- and four-temperature cycles is that in the latter, waste heat is supplied at two intermediate temperatures instead of one, as in the former. The trend of the results is the same as in Fig. 8. The alloys have to be operated at low cycle times (3-6 min) to be viable for heat pump applications.

In absorption beds of the solid-vapor type, decreasing the cycle time is a very difficult problem to overcome because of the limitations imposed by material properties and bed characteristics. According to the standards of current technology, cycle times of less than 20 min are difficult to achieve. This limitation forces the material inventory to increase, thereby adversely affecting costs.

To determine the factors influencing cycle times, the mass transfer zone (MTZ) concept is used to describe the rate of absorption and heat transfer in fixed-bed absorption systems. First the pertinent features of this model are described and later, the design equations are presented.

6. ADSORPTION BED DESIGN PARAMETERS

6.1 The Mass Transfer Zone (MTZ) Concept

Consider a fixed bed containing an adsorbent with a feed stream entering on the left as shown in Fig. 10. Initially, the adsorbent is highly activated with a low adsorbate loading, x_o [Fig. 10(a)]. If the feed gas flow is started at time $\theta = 0$, then as the gas flows through the bed it will be absorbed by the adsorbent. At some later time, $\theta > 0$, an analysis of the adsorbent samples taken at various cross-sections of the bed would show an adsorbate loading curve as in Fig. 10(b). At the bed inlet, under steady-state conditions, the equilibrium loading would be x_e corresponding to the maximum capacity of the adsorbate (hydride) to absorb H_2 at its given H/M ratio. The portion of the bed whose adsorbate loading is equal to x_e is called the equilibrium zone.

Toward the outlet side of the bed, essentially no gas will emerge initially and the loading of the bed would be equal to the initial loading, $x_o \approx 0$. This portion is known as the unused bed.

In some intermediate zone between the equilibrium zone and the unused bed, the adsorbate loading will be as shown in Fig. 10(c). It is in this zone that the gas is being transported from the feed stream into the adsorbent bed, and is called the mass transfer zone (MTZ). The inverse S-shaped wave in the MTZ is called the mass transfer wave or front.

As flow continues under steady-state conditions, the MTZ moves further to the right at a uniform velocity. Breakthrough occurs when the leading edge of the MTZ just leaves the outlet end of the bed, at time $\theta = \theta_b$, as shown in Fig. 10(d). The time taken for the front to travel the entire length of the bed until breakthrough occurs is called the breakthrough time, θ_b .

If the flow of gas at the inlet is continued, the adsorbent loading curve will look as in Figs. 10(e) and 10(f) and finally when $\theta > \theta_e$ the entire bed is at its equilibrium loading, the curve will appear as in Fig. 10(g) and no further absorption will occur.

6.2 Design Equations

6.2.1 Mass transfer

The mass of hydrogen gas absorbed in time θ to $\theta + \Delta\theta$ is,

$$w = G_s A \Delta\theta \quad (7)$$

The mass of hydrogen transferred in the MTZ is:

$$w = (x_i - x_o) A L_f \rho_b \quad (8)$$

Equate Eqs. 7 and 8 to solve for mass transfer wave length, or front

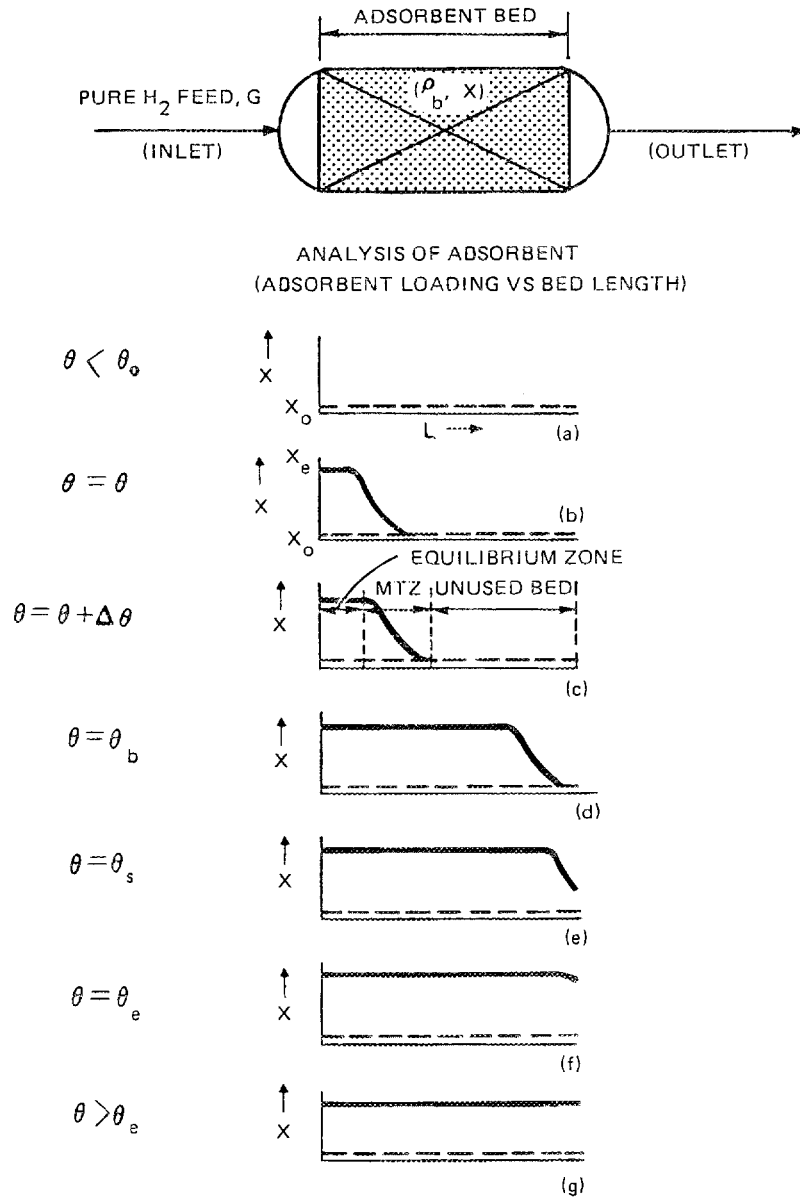


Fig. 10. Mass transfer zone (MTZ) and adsorbate loading curves during various stages of absorption.

length, L_f :

$$L_f = \frac{G_s \Delta\theta}{(x_i - x_o)\rho_b} . \quad (9)$$

But

$$L_f = v_f \Delta\theta , \quad (10)$$

where v_f is the front velocity.

From Eqs. 9 and 10,

$$v_f = \frac{G_s}{(x_i - x_o)\rho_b} . \quad (11)$$

It is important to point out that the front velocity, v_f , is only a function of the boundary conditions of the adsorbent bed. By this it is meant that the conditions existing at the inlet and outlet section of the bed determine uniquely the velocity. The bulk density ρ_b has the same value at the boundary as it has within the bed.

6.2.2 Heat transfer

The heat generated in the MTZ due to absorption of hydrogen gas is,

$$Q = G_s A \Delta H . \quad (12)$$

For isothermal operation, this quantity of heat must be removed by circulating a cooling medium around the bed walls. The transfer of heat therefore occurs transverse to the flow of feed gas. The heat transfer rate per unit volume of the absorption bed is given by,^{2,7}

$$\frac{qR}{4k_a} + \frac{qR}{2k_t} \left[\frac{k_t}{R_1 h_a} + \ln \frac{R_1}{R} \right] = T_1 - T_0 . \quad (13)$$

If the tube material is thin, $R_1 = R$ and $\ln(R_1/R) = 0$. With this simplification, Eq. 13 reduces to,

$$qR^2 \left[\frac{1}{4k_a} + \frac{1}{2Rh_a} \right] = (T_1 - T_0) = \Delta T . \quad (14)$$

Taking the Least Common Multiple (LCM) of the term within the square brackets on the left-hand side of Eq. 14 and simplifying gives,

$$q = \frac{4k_a h_a R \Delta T}{R^2 [Rh_a + 2k_a]} . \quad (15)$$

But

$$q = Q\pi R^2 L . \quad (16)$$

Equating Eqs. 15 and 16 gives,

$$Q = \frac{4k_a h_a R\pi L}{[Rh_a + 2k_a]} \Delta T . \quad (17)$$

But $h_a \gg k_a$. Therefore,

$$Q = 4\pi L k_a \Delta T . \quad (18)$$

Equating Eqs. 18 and 12 gives,

$$4\pi L k_a \Delta T = G_s A \Delta H . \quad (19)$$

If the length of tube considered is equal to one front length, L_f , and since $A = \pi R^2 = (\pi D^2)/4$, Eq. 19 becomes

$$L_f = \frac{G_s D^2 \Delta H}{16k_a (\Delta T)} . \quad (20)$$

Equating Eqs. 20 and 9 for L_f gives an equation for the time it takes the mass transfer wave to travel one front length.

$$\Delta\theta = \Delta\theta_f = \frac{D^2 (x_i - x_o) \rho_b \Delta H}{16k_a (\Delta T)} . \quad (21)$$

In actual fixed-bed absorption operation, the cycle time is three to four times $\Delta\theta_f$ to allow sufficient time for the inverse S-shaped mass transfer wave profile to develop and attain steady state.

The factors which determine the cycle time are evident from Eq. 21. Lower values of $\Delta\theta_f$ (and consequently lower cycle times) can be attained by increasing the denominator and reducing the numerator of Eq. 21. However, ρ_b , x_i , x_o , and ΔH are properties of the bed material and are constant. Therefore, D , k_a , and ΔT can be varied. D is the diameter of each adsorbent-filled tube comprising the bed. The smaller the

diameter, D , of each tube, the larger the number of tubes required, which increases the costs. Moreover, the commercial manufacture of tubes below a certain diameter becomes too expensive. The thermal conductivity of the adsorbent bed material, k_a , can be increased by tightly packing the material together,* but there is a certain void fraction which cannot be transcended. Moreover, the hydrides expand during hydrogen absorption which increases the voidage, and somewhat lowers k_a . The only easily varied quantity happens to be ΔT , the difference in temperature between the adsorbent bed and the cooling fluid circulating outside. For steam production, the temperature of the cooling fluid must be high. Therefore, ΔT cannot be too great, otherwise the required process steam temperatures will never be reached.

The norm in pilot size units^{†,9} have a cycle time of about 20 min. If k_a can be improved by 10% and ΔT by 20%, then the overall reduction in cycle time using Eq. 22 can be shown to be 32%. The average cycle time of 20 min can then be reduced to 13.6 min. However, to be economically viable, the cycle times must be at least 5 min, if not less, and the hydride material must endure for two years without requiring partial or complete replacement.

* A report⁸ by SRI International mentions a process developed by Daimler-Benz that improves thermal conductivity by a factor of 10 to 30 when certain hydrides are mixed with 5-20 wt % of metals such as aluminum, magnesium, and copper. The important point to note is that in a hydride bed, the empty spaces between hydride pellets have a deteriorating effect on the bed thermal conductivity which predominates over the contribution to the bed thermal conductivity made by the solid hydride material. Nickel has been traditionally used as support material for hydrides because of its spiky structure which is ideally suited for formation of a porous pellet following sintering and heat treatment. The quality of pellet material produced by using aluminum, magnesium, and copper is uncertain. The increase in thermal conductivity by a factor of 10 to 30 seems a little high because the thermal conductivities of nickel, aluminum, magnesium, and copper are approximately in the ratio of 1:3:2.5:7. Therefore, if all the nickel support previously used was replaced by copper, the thermal conductivity of the particle would be increased by a factor of 7. However, as pointed out earlier, the main obstacle in improving bed thermal conductivity is the void fraction.

[†] There are no commercial hydride units available. A pilot-scale unit at Air Products Company, designed to recover hydrogen from an ammonia slipstream, is the closest current approximation to a commercial unit and is the only one of its kind known to exist in the United States.

7. CYCLIC STABILITY, DECREPITATION, KINETICS AND COSTS

7.1 Stability

The most exhaustive literature survey and laboratory data collection on hydride materials was recently completed by Ergenics, Inc.² The following are excerpts from this report.

Even in the absence of any impurities, intermetallic hydriding alloys can be degraded during repeated cycling by separation, or disproportionation, of the metal species. This is because many of the alloys are thermodynamically metastable in respect to the hydride of the most reactive component.

A dramatic example of this occurs with the alloy CaNi_5 which would otherwise be an important alloy due to its good capacity and low cost. However, it can lose much of its hydrogen absorption capacity in less than 300 cycles at 85°C (185°F).¹⁰ This loss can be reversed, but the inconvenience diminishes the alloy's use. On the other hand, the problem appears to be avoided by alloy selection. Compounds based on $\text{La}(\text{Ni},\text{Al})_5$ are found to be essentially immune to this intrinsic disproportionation.¹⁰

A possibly related cyclic instability is known to occur in some AB type compounds. In this case it is more likely a disordering phenomenon and it affects ZrCo ¹¹ and the dihydride (upper) plateau of some alloys based on TiFe .

7.2 Decrepitation

Volume expansion occurs during the hydriding reaction which can range from 10 to 25%. Most of the alloys are quite brittle, crack severely on expansion, and decrepitate to fine powder within a few absorption and desorption cycles. The fine powder state is a mixed blessing. It provides high surface area which can help reaction kinetics and getter impurities. On the other hand, it packs in reactors causing increased pressure drops and container bulging. The fine powder also results in poor heat transfer, and some alloys in this state can be very pyrophoric.

The handling of the fine alloy powders has led to several containment approaches. These include permeable capsules¹² and bonded pellets. The latter approach can include improved management of the reaction heating and cooling by enhancing thermal conductivity or by thermal ballast. Pellet porosity can affect gas flow, and different alloys could have varying sensitivity to the binders that may be used to make pellets.

7.3 Reaction Kinetics

Intrinsic reaction rate constants for the hydriding reactions are functions of temperature and pressure. These functions suggest an optimum pressure and temperature combination for maximum absorption reaction rate.¹³

With the exception of magnesium alloys, the intrinsic kinetics of hydriding reactions for most alloys appears to be so rapid that operation of practical devices is usually controlled by other factors. The principal factors are heat transfer, gas permeability, and impurity effects. Unfortunately, these (and pressure dependence) are often overlooked in determinations and analyses of kinetics reported in the literature. The data in most reports are so uncertain that they cannot be used in connection with alloy selection.

7.4 Cost and Availability

There are many intermetallic hydriding alloys in the literature that are composed of very exotic and expensive elements. No one, for example, would consider using thorium, hafnium, gadolinium, etc., on a large scale in an industrial process. Even so, many of the metals included are expensive: Zr, La, Ti, and Co are examples; Ni, which is contained in many compositions, is lower in cost but hardly inexpensive. In addition, many of the alloys require special techniques or care in preparation and this adds to cost.

Nevertheless, the generally unavoidable, relatively high materials costs can be balanced in several ways. Expensive lanthanum is diluted 1:5 with nickel, and/or is replaced with less expensive mischmetal. Iron and manganese which are less expensive are used where possible. Finally, alloys with high hydrogen capacity are used where possible, and they are cycled as rapidly as practicable to minimize the quantity that a process must have in inventory. These considerations all become part of the alloy selection process and economic basis of any process development.

REFERENCES

1. Ally, M. R., et al., "Metal Hydride Chemical Heat Pumps for Industrial Use," 1984 IECTCE, Houston, Texas, April 15-18, 1984.
2. Goodall, P. D., "Energy Conservation Using Metal Hydrides for Hydrogen Recovery and Steam Generation from Industrial Waste Gas Streams," DOE Contract DE-AC07-84ID12520 (in publication).
3. Sandrock, G. D., and Huston, E. L., "How metals store hydrogen," *CHEMTECH*, Vol. 11, pp. 754-62 (1981).
4. Snape, E., and Lynch, F. E., "Metal hydrides make hydrogen accessible-1," *CHEMTECH*, Vol. 10, pp. 578-83 (1980).
5. Raldow, W. M., and Wentworth, W. E., "Chemical Heat Pumps--A Basic Thermodynamic Analysis," *Solar Energy*, Vol. 23, pp. 75-79 (1979).
6. Southern California Gas Company, Metal Hydride/Chemical Heat Pump Development Project, Phase I Final Report, Contract 534098-S, February 1982.
7. Personal communication with P. D. Goodell, Ergenics, Inc., Wyckoff, New Jersey.
8. Argabright, T. A., *Metal Hydride Heat Pump Development Project*, BNL 51539, February 1982.
9. Air Products and Chemicals, Inc., Allentown, PA.
10. Goodell, P. D., Sandrock, G. D., and Bogdanski, R. R., *Cyclic Hydrogen Transfer and Adsorption/Poisoning Tests of AB and AB₅ type Hydriding Alloys. Final Report*, ed. E. L. Huston, BNL 35440-Vol. II, BNL 509926-S, Brookhaven National Laboratory, 1984.
11. Irving, S. J. C., and Harris, I. R., "The Effect of Induced Disorder on the Hydrogenation Behaviors of the Phase ZrCo," pp. 431-440 in *Hydrides for Energy Storage. Proceedings of the International Symposium, Giels, Norway, 1978*.
12. Truillon, P. P., and Sandrock, G. D., "Hydrogen Container," U. S. Patent 4,133,426, Jan. 9, 1979.
13. Suda, S., Kobayashi, N., and Yoshida, K., "Reaction Kinetics of Metal Hydrides and Their Mixtures," *J. Less-Common Metals*, Vol. 73, pp. 119-26 (1980).

APPENDIX

LISTING AND EXECUTION OF COMPUTER PROGRAM, HYDRIDE

```

C   COMPUTER PROGRAM ENABLES USER TO DESIGN A SINGLE STAGE METAL
C   HYDRIDE TEMPERATURE AMPLIFIER MACHINE.
C
C
10  WRITE(6,20)
20  FORMAT(1X,'THE FOLLOWING METAL HYDRIDES ARE CONSIDERED:',/,
      1 ' 1. ZIRCONIUM-COBALT, ZRCO',/,
      2 ' 2. ZIRCONIUM-NICKEL, ZRNI',/,
      3 ' 3. MAGNESIUM-NICKEL, MG2NI',/,
      4 ' 4. TITANIUM-MIDKEL, TI2NI',/,
      5 ' 5. TITANIUM-VANADIUM-CABALT,TI0.95V0.05CO',/,
      6 ' 6. TITANIUM-CABALT, TICO',/,
      7 ' 7. TITANIUM-COBALT-MANGANESE, TICO0.5MN0.5',/,
      8 ' 8. TITANIUM-IRON-NICKEL-VANADIUM,TIFE0.8NI0.1V0.05',/,
      9 ' 9. TITANIUM-IRON-NICKEL, TUFE0.8NI0.2',/,
      C '(THE ABOVE INCLUDE A,A2B,AND AB TYPE ALLOYS)')
30  WRITE(6,40)
40  FORMAT(1X,'CHOOSE HOT AND CLOD SIDE ALLOYS ACCORDING TO ABOVE
      C NUMBERING SYSTEM')
      WRITE(6,60)
60  FORMAT(2X,'HOT SIDE ALLOY, HOTA = ')
      READ(5,65)HOTA
65  FORMAT(2X,F5.1)
      WRITE(6,90)
90  FORMAT(2X,'COLD SIDE ALLOY, COLDA = ')
      READ(5,95)COLDA
95  FORMAT(2X,F5.1)

C
      WRITE(6,110)
110  FORMAT(2X,'WASTE HEAT TEMP. FOR HOT SIDE ALLOY, F= ')
      READ(5,115)TWH
115  FORMAT(2X,F5.1)
      TWHK=KELVN(TWH)
      DEGC=DEGK2C(TWHK)
C   WRITE(11,117)HOTA,COLDA,TWH,TWHK
117  FORMAT(2X,'HOTA =',F3.1,'COLDA =',F3.1,'TWH =',F5.1,'TWHK',F5.1)
C
      CALL VANTHF(HOTA,TWHK,PR)
      PH1=PR
      DELTAP=0.0
      PC1=PH1-DELTAP
      CALL HFVANT(COLDA,PC1,TC)
C   WRITE(6,900)TC
900  FORMAT(2X,'TC VALUE FROM HFVANT (K)= ',F7.1,/)
      T=TC
      TC1F=FAREN(T)
      T=TC1F
      TC1K=KELVN(T)
      T=TC1K
      TC1C=DEGK2C(T)
C   WRITE(11,119)PH1,TC,T
119  FORMAT(' PH1=',F8.5,' TC(F) =',F7.1,' T =',F7.1)
      IF(TC.GE.TWHK)GO TO 120

```

```

        GO TO 140
120  WRITE(6,130)
130  FORMAT(2X,'WRONG SELECTION OF COLD SIDE ALLOY'])
140  CONTINUE
        WRITE(6,150)
150  FORMAT(2X,'WASTE HEAT TEMP. FOR COLD SIDE ALLOY, F =')
        READ(5,160)TWCA
160  FORMAT(2X,F5.1)
        TWCA=KELVN(TWCA)
        CALL VANTHF(COLDA,TWCA,PR)
        PC2=PR
        T=TWCA
        TC2F=FAREN(T)
        T=TC2F
        TC2K=KELVN(T)
        T=TC2K
        TC2C=DEGK2C(T)
        DELPC=0.0
        PH2=PC2-DE LPC
        CALL HFVANT(HOTA,PH2,TC)
        T=TC
        TH2F=FAREN(T)
        T=TH2F
        TH2K=KELVN(T)
        T=TH2K
        TH2C=DEGK2C(T)
        WRITE(6,170)
170  FORMAT(2X,'DESIRED HEAT PUMP CAPACITY(BTU/HR = IN E9.1 FORMAT')
        READ(6,180)BTU
180  FORMAT(2X,E9.1)
C
        CALL DELTAH(HOTA,DELH)
        DHBTU=CALBTU(DELH)*454.0
C
C  WRITE(6,190)DHBTU
190  FORMAT(2X,/, 'DHBTU = ',F8.1,/)
C
C  LB-MOLES/HR OF HYDROGEN REQUIRED
C
        REQDH2=BTU/DHBTU
C
        WRITE(6,200)
200  FORMAT(2X,'H/M RATIO FOR HOT ALLOY = ')
        READ(5,210)HMHOT
210  FORMAT(2X,F3.2)
        WRITE(6,250)
250  FORMAT(2X,'H.M RATIO FOR COLD ALLOY =')
        READ(5,260)HMCOLD
260  FORMAT(2X,F3.2)
C
        CALL LBATOM(HOTA,POUNDA)
C  LB ALLOY PER LB HYDROGEN, H2HOT
        H2HOT=POUNDA/HMHOT
        CALL LBATOM(COLDA,POUNDA)

```

```

C   LB COLD ALLOY PER LB HYDROGEN
      H2COLD=POUNDA/HMCOLD
C
C
      WRITE(6,220)
220  FORMAT(2X,'CYCLE TIME (IN MINUTES) ? ')
      READ(5,230)CYCLE
230  FORMAT(2X,F5.1)
C
C   LB-MOLES H2 ABSORBED IN EACH CYCLE, H2ABS
      H2ABS=REQDH2*CYCLE/60.
C
C   ALLOY (HOT) INVENTORY PER BED QHALOI(LB ALLOY)
      QHALOI=H2ABS*2.0*H2HOT
      CALL COPTA(HOTA,COLDA,COP)
C
C   ALLOY (COLD) INVENTORY PER BED, QCALOI
      QCALOI=H2ABS*H2COLD
C
C
      CALL PRINT(TWH,DEGC,TWHK,PH1,PC1,TC1F,TC1C,TC1K,PC2,TC2F,TC2C,
C TC2K,PH2,TH2F,TH2C,TH2K)
C
C
      CALL PRINT1(BTU,DHBTU,HMHOT,H2HOT,CYCLE,H2ABS,QHALOI,HMCOLD,
C H2COLD,QCALOI)
      WRITE(6,240)COP
240  FORMAT(/,2X,'COP',14X,F5.2,/)
C
      STOP
      END
C
C
      FUNCTION P1(T)
C   EQ. PRESSURE OF H2 ABOVE HYDRIDE
      P1=10**(-4137/T+6.486)
      RETURN
      END
C
C
      FUNCTION P2(T)
C   EQ. PRESSURE OF HYDROGEN OVER HYDRIDE
      P2=10**(-4025/T+7.075)
      RETURN
      END
C
C
      FUNCTION P3(T)
C   EQ PRESSURE OF H2 OVER MG2NI
      P3=10**(-3534/T+6.730)
      RETURN
      END
C
C

```

```
FUNCTION P4(T)
C EQ. PRESSURE OF H2 OVER TI2NI
  P4=10**(-3578/T+7.434)
  RETURN
  END
C
C
FUNCTION P5(T)
C EQ. PRESSURE OF H2 OVER TI0.95V0.05CO
  P5=10**(-4221/T+9.733)
  RETURN
  END
C
C
FUNCTION P6(T)
C EQ. PRESSURE OF H2 OVER TICO
  P6=10**(-3204/T+7.993)
  RETURN
  END
C
C
FUNCTION P7(T)
C EQ. PRESSURE OF H2 OVER TICO0.5MN0.5
  P7=10**(-2412/T+6.604)
  RETURN
  END
C
C
FUNCTION P8(T)
C EQ. PRESSURE OF H2 OVER TIFE0.8NI0.15V0.05
  P8=10**(-2297/T+6.358)
  RETURN
  END
C
C
FUNCTION P9(T)
C EQ. PRESSURE OF H2 OVER TIFE0.8NI0.2
  P9=10**(-2.199/T+6.324)
  RETURN
  END
C
C
FUNCTION TC1(P)
  TC1=4137/(6.486-ALOG10(P))
  RETURN
  END
C
C
FUNCTION TC2(P)
  TC2=4025/(7.075-ALOG10(P))
  RETURN
  END
C
C
```

```
FUNCTION TC3(P)
TC3=3534/(6.730-ALOG10(P))
RETURN
END
C
FUNCTION TC4(P)
TC4=3578/(7.434-ALOG10(P))
RETURN
END
C
FUNCTION TC5(P)
TC5=4221/(9.733-ALOG10(P))
RETURN
END
C
FUNCTION TC6(P)
TC6=3204/(7.993-ALOG10(P))
RETURN
END
C
FUNCTION TC7(P)
TC7=2412/(6.604-ALOG10(P))
RETURN
END
C
FUNCTION TC8(P)
TC8=2297/(6.358-ALOG10(P))
RETURN
END
C
FUNCTION TC9(P)
TC9=2199/(6.324-ALOG10(P))
RETURN
END
C
FUNCTION KELVN(T)
KELVN=(T+460)/1.8
RETURN
END
C
C
FUNCTION FAREN(T)
FAREN=T*1.8-460.
RETURN
END
C
C
FUNCTION DEGK2C(T)
DEGK2C=T-273.0
RETURN
END
C
C
FUNCTION BTU2W(B)
```

```

      BTU2W=0.293*B
      RETURN
      END
C
C
      FUNCTION CALBTU(C)
      CALBTU=1/252.*C
      RETURN
      END
C
C
      FUNCTION CALJUL(CJ)
      CALJUL=4.186*CJ
      RETURN
      END
      SUBROUTINE DELTAH(ALOI,DELH)
      R=1.987
      E=2.303
      IF(ALOI.EQ.1)GO TO 10
      IF(ALOI.EQ.2)GO TO 20
      IF(ALOI.EQ.3)GO TO 30
      IF(ALOI.EQ.4)GO TO 40
      IF(ALOI.EQ.5)GO TO 50
      IF(ALOI.EQ.6)GO TO 60
      IF(ALOI.EQ.7)GO TO 70
      IF(ALOI.EQ.8)GO TO 80
      IF(ALOI.EQ.9)GO TO 90
      CONTINUE
10  DELH=4137*R*E
      GO TO 100
20  DELH=4025*R*E
      GO TO 100
30  DELH=3534*R*E
      GO TO 100
40  DELH=3578*R*E
      GO TO 100
50  DELH=4221*R*E
      GO TO 100
60  DELH=3204*R*E
      GO TO 100
70  DELH=2412*R*E
      GO TO 100
80  DELH=2297*R*E
      GO TO 100
90  DELH=2199*R*E
100 RETURN
      END
      SUBROUTINE VANTHF(ALOI,T,PR)
C
C
      IF(ALOI.EQ.1)GO TO 10
      IF(ALOI.EQ.2)GO TO 20
      IF (ALOI.EQ.3)GO TO 30
      IF(ALOI.EQ.4)GO TO 40

```

```

        IF(ALOI.EQ.5)GO TO 50
        IF(ALOI.EQ.6)GO TO 60
        IF(ALOI.EQ.7)GO TO 70
        IF(ALOI.EQ.8)GO TO 80
        IF(ALOI.EQ.9)GO TO 90
        CONTINUE
10  PR=P1(T)

        GO TO 100
20  PR=P2(T)
        GO TO 100
30  PR=P3(T)
        GO TO 100
40  PR=P4(T)
        GO TO 100
50  PR=P5(T)
        GO TO 100
60  PR=P6(T)
        GO TO 100
70  PR=P7(T)
        GO TO 100
80  PR=P8(T)
        GO TO 100
90  PR=P9(T)
        GO TO 100
100 RETURN
    END
    SUBROUTINE HFVANT(ALOI,P,TC)
        IF(ALOI.EQ.1)GO TO 10
        IF(ALOI.EQ.2)GO TO 20
        IF(ALOI.EQ.3)GO TO 30
        IF(ALOI.EQ.4)GO TO 40
        IF(ALOI.EQ.5)GO TO 50
        IF(ALOI.EQ.6)GO TO 60
        IF(ALOI.EQ.7)GO TO 70
        IF(ALOI.EQ.8)GO TO 80
        IF(ALOI.EQ.9)GO TO 90
        CONTINUE
10  TC=TC1(P)
        GO TO 100
20  TC=TC2(P)
C   WRITE(6,911)ALOI,P,TC
911  FORMAT(2X,'VALUES FROM HFVANT: ',/,
        C 2X,'ALOI=',F5.1,' P(ATM)= ',F8.4,' TC(K) =',F7.1)
        GO TO 100
30  TC=TC3(P)
        GO TO 100
40  TC=TC4(P)
        GO TO 100
50  TC=TC5(P)
        GO TO 100
60  TC=TC6(P)
        GO TO 100
70  TC=TC7(P)

```

```

      GO TO 100
80  TC=TC8(P)
      GO TO 100
90  TC=TC9(P)
      GO TO 100
100 RETURN
      END

```

C
C

```

      SUBROUTINE LBATOM(ALOI,POUNDA)
      IF(ALOI.EQ.1)GO TO 10
      IF(ALOI.EQ.2)GO TO 20
      IF(ALOI.EQ.3)GO TO 30
      IF(ALOI.EQ.5)GO TO 50
      IF(ALOI.EQ.6)GO TO 60
      IF(ALOI.EQ.7)GO TO 70
      IF(ALOI.EQ.8)GO TO 80
      IF(ALOI.EQ.9)GO TO 90
10  POUNDA=75.0
      GO TO 100
20  POUNDA=74.95
      GO TO 100
30  POUNDA=35.78
      GO TO 100
40  POUNDA=51.50
      GO TO 100
50  POUNDA=53.50
      GO TO 100
60  POUNDA=53.42
      GO TO 100
70  POUNDA=52.42
      GO TO 100
80  POUNDA=51.97
      GO TO 100
90  POUNDA=52.16
100 RETURN
      END
      SUBROUTINE COPTA(HOTA,COLDA,COP)
      CALL DELTAH(HOTA,DELHOT)
      CALL DELTAH(COLDA,DELCLD)
      COP=DELHOT/(DELHOT+DELCLD)
      RETURN
      END
      SUBROUTINE PRINT(TWH,DEGC,TWHK,PH1,PC1,TC1F,TC1C,TC1K,PC2,TC2F,
C TC2C,TC2K,PH2,TH2F,TH2C,TH2K)
C
      WRITE(6,170)TWH,DEGC,TWHK
170  FORMAT(1X,/,,'WASTE HEAT SOURCE TEMP. FOR HOT SIDE ALLOY ',F7.1,
C '(F)',F7.1,'(C)',F7.1,'(K)',/)
      WRITE(6,180)PH1
180  FORMAT(1X,'HOT SIDE ALLOY (LOW PRESSIRE),ATM ',11X,F8.4,/)
      WRITE(6,190)PC1
190  FORMAT(1X,'COLD SIDE ALLOY (LOW PRESSURE),ATM ',10X,F8.4,/)
      WRITE(6,200)TC1F,TC1C,TC1K

```

```

200 FORMAT(1X,'COLD SIDE ALLOY (LOW TEMPERATURE) ',11X,F7.1,'(F)',
      C F7.1,'(C)',F7.1,'(K)',/)
220 FORMAT(1X,'WASTE HEAT SOURCE TEMP. FOR COLD SIDE ALLOY ',F7.1,
      C '(F)',F7.1,'(C)',F7.1,'(K)',/)
      WRITE(6,210)PC2
210 FORMAT(1X,'COLD SIDE ALLOY (HIGH PRESSURE), ATM ',8X,F8.4,/)
      WRITE(6,220)TC2F,TC2C,TC2K
      WRITE(6,230)PH2
230 FORMAT(1X,'HOT SIDE ALLOY (HIGH PRESSURE), ATM ',10X,F8.4,/)
      WRITE(6,240)TH2F,TH2C,TH2K
240 FORMAT(1X,'HOT SIDE ALLOY (HIGH TEMPERATURE) ',11X,F7.1,'(F)',
      C F7.1,'(C)',F7.1,'(K)',/)
      RETURN
      END

C
      SUBROUTINE PRINT1(BTU,DHBTU,HMHOT,H2HOT,CYCLE,H2ABS,QHALOI,
      C HMCOLD,H2COLD,QCALOI)
      WRITE(6,250)BTU,DHBTU,HMHOT,H2HOT,CYCLE,H2ABS,QHALOI,
      C HMCOLD,H2COLD,QCALOI
250 FORMAT(/,2X,'DESIRED CHP CAPACITY,BTU/HR = ',12X,E9.1,/,
      C 2X,'HEAT OF ABSORPTION,BTU/LB-MOLE = ',10X,F8.1,/,
      C 2X,'HYDROGEN TO METAL ATOM RATIO (HOT ALLOY) = ',F3.1,/,
      C 2X,'LB ALLOY (HOT)/LB H2 = ',18X,F8.1,/,
      C 2X,'CYCLE TIME, MINS = ',24X,F5.1,/,
      C 2X,'LB HYDROGEN ABSORBED PER CYCLE = ',6X,F8.1,/,
      C 2X,'LB ALLOY (HOT) IN EACH BED = ',13X,F8.1,/,
      C 2X,'HYDROGEN TO METAL ATOM RATIO (COLD ALLOY) = ',F3.1,/,
      C 2X,'LB ALLOY (COLD)/LB OF H2 = ',14X,F8.1,/,
      C 2X,'LB ALLOY (COLD) IN EACH BED = ',13X,F8.1)
      RETURN
      END

```

EX
 LINK: Loading
 [LNKXCT HYDRID execution]

THE FOLLOWING METAL HYDRIDES ARE CONSIDERED:

1. ZIRCONIUM-COBALT, ZRCO
2. ZIRCONIUM-NICKEL, ZRNI
3. MAGNESIUM-NICKEL, MG2NI
4. TITANIUM-MIDKEL, TI2NI
5. TITANIUM-VANADIUM-CABALT, TI0.95VO.05CO
6. TITANIUM-CABALT, TICO
7. TITANIUM-COBALT-MANGANESE, TICOO.5MNO.5
8. TITANIUM-IRON-NICKEL-VANADIUM, TIFE0.8NIO.1VO.05
9. TITANIUM-IRON-NICKEL, TUFE0.8NIO.2

THE ABOVE INCLUDE A,A2B,AND AB TYPE ALLOYS)
 CHOOSE HOT AND CLOD SIDE ALLOYS ACCORDING TO ABOVE NUMBERING SYSTEM

HOT SIDE ALLOY, HOTA =

3.0

COLD SIDE ALLOY, COLDA =

5.0

WASTE HEAT TEMP. FOR HOT SIDE ALLOY, F=

325.0

WASTE HEAT TEMP. FOR COLD SIDE ALLOY, F =

325.0

DESIRED HEAT PUMP CAPACITY(BTU/HR = IN E9.1 FORMAT

30.0E06

H/M RATIO FOR HOT ALLOY =

0.2

H.M RATIO FOR COLD ALLOY =

0.2

CYCLE TIME (IN MINUTES) ?

20.0

ASTE HEAT SOURCE TEMP. FOR HOT SIDE ALLOY	325.0(F)	163.0(C)	436.0(K)
HOT SIDE ALLOY (LOW PRESSURE), ATM	0.0421		
COLD SIDE ALLOY (LOW PRESSURE), ATM	0.0421		
COLD SIDE ALLOY (LOW TEMPERATURE)	224.0(F)	106.0(C)	379.0(K)
COLD SIDE ALLOY (HIGH PRESSURE), ATM	1.1267		
WASTE HEAT SOURCE TEMP. FOR COLD SIDE ALLOY	324.8(F)	163.0(C)	436.0(K)
HOT SIDE ALLOY (HIGH PRESSURE), ATM	1.1267		
HOT SIDE ALLOY (HIGH TEMPERATURE)	492.5(F)	256.0(C)	529.0(K)

DESIRED CHP CAPACITY, BTU/HR =	0.3E+08
HEAT OF ABSORPTION, BTU/LB-MOLE =	29134.9
HYDROGEN TO METAL ATOM RATIO (HOT ALLOY) =	.2
LB ALLOY (HOT)/LB H2 =	178.9
CYCLE TIME, MINS =	20.0
LB HYDROGEN ABSORBED PER CYCLE =	343.2
LB ALLOY (HOT) IN EACH BED =	122808.0
HYDROGEN TO METAL ATOM RATIO (COLD ALLOY) =	.2
LB ALLOY (COLD)/LB OF H2 =	267.5
LB ALLOY (COLD) IN EACH BED =	91814.3

COP 0.46

STOP

END OF EXECUTION

CPU TIME: 0.27 ELAPSED TIME: 44.17

EXIT

INTERNAL DISTRIBUTION

- | | |
|--------------------|---------------------------------|
| 1-3. M. R. Ally | 18. F. C. Maienschein |
| 4. V. D. Baxter | 19. J. F. Martin |
| 5. J. Braunstein | 20. S. H. McConathy |
| 6. R. S. Carlsmith | 21. H. A. McLain |
| 7. R. C. DeVault | 22. V. C. Mei |
| 8. N. Domingo | 23. M. R. Patterson |
| 9. P. D. Fairchild | 24. H. Perez-Blanco |
| 10. S. K. Fischer | 25. C. K. Rice |
| 11. B. J. Frame | 26. T. J. Wilbanks |
| 12. W. Fulkerson | 27-28. Central Research Library |
| 13. L. D. Gilliam | 29. Document Reference Section |
| 14. W. R. Huntley | 30. Laboratory Records--RC |
| 15. S. I. Kaplan | 31-32. Laboratory Records |
| 16. J. O. Kolb | 33. ORNL Patent Section |
| 17. M. A. Kuliasha | |

EXTERNAL DISTRIBUTION

34. W. Bierman, 45 Foxcroft Drive, Fayetteville, NY 13066
35. J. M. Calm, Electric Power Research Institute, 3412 Hillview Avenue, P.O. Box 10412, Palo Alto, CA 94303
36. Jaime G. Carbonell, Associate Professor of Computer Science, Carnegie-Mellon University, Pittsburgh, PA 15213
37. G. Douglas Carver, TVA, 703 Power Building, Chattanooga, TN 37402
38. R. N. Chappell, Program Manager, Energy Conservation Branch, Energy and Technology Division, DOE Idaho Operations Office, 785 DOE Place, Idaho Falls, ID 83402
39. D. C. Erickson, Energy Concepts Company, 627 Ridgely Avenue, Annapolis, MD 21401
40. R. J. Fiskum, Program Manager, Energy Conversion Equipment Branch, CE-132, Room GH-068, FORSTL, Department of Energy, 1000 Independence Avenue SW, Washington, DC 20585
41. Joel Gilbert, Dames and Moore, Inc., 7101 Wisconsin Avenue, Suite 700, Bethesda, MD 20814
42. S. Malcolm Gillis, Professor, Public Policy and Economics, Duke University, 4875 Duke Station, Durham, NC 27706
43. G. Grossman, Technion Institute of Technology, Faculty of Mechanical Engineering, Haifa, Israel
44. W. T. Hanna, Battelle Columbus Laboratories, 505 King Avenue, Columbus, OH 43201
45. F. C. Hayes, Trane Company, 3600 Pammel Creek Road, LaCrosse, WI 54601

46. Fritz R. Kalhammer, Vice President, Electric Power Research Institute, P.O. Box 10412, Palo Alto, CA 94303
47. Alan Karp, Electric Power Research Institute, Energy Management and Utilization Division, P.O. Box 10412, Palo Alto, CA 94303
48. R. E. Kasperson, Professor of Government and Geography, Graduate School of Geography, Clark University, Worcester, MA 01610
49. M. Lessen, Consulting Engineer, 12 Country Club Drive, Rochester, NY 14618
50. R. Macriss, Institute of Gas Technology, 3424 South State Street, Chicago, IL 60616
51. L. A. McNeely, 7310 Steinmeier Drive, Indianapolis, IN 46250
52. D. K. Miller, Borg-Warner Air Conditioning, Inc., P.O. Box 1592, York, PA 17405
53. J. I. Mills, EG&G Idaho, Inc., P.O. Box 1625-WCB, Idaho Falls, ID 83415
54. B. A. Phillips, Phillips Engineering Company, 721 Pleasant Street, St. Joseph, MI 49085
55. R. Radermacher, University of Maryland, Mechanical Engineering Department, College Park, MD 20742
56. W. J. Rebello, PAR Enterprises, 11928 Appling Valley Road, Fairfax, VA 22030
57. R. C. Reimann, 5504 Ortloff Road, LaFayette, NY 13084
58. S. L. Richlen, Office of Industrial Programs, CE-141, FORSTL, Department of Energy, 1000 Independence Avenue SW, Washington, DC 20585
59. J. D. Ryan, Energy Conversion Equipment Branch, CE-132, FORSTL, Department of Energy, 1000 Independence Avenue SW, Washington, DC 20585
60. U. Rockenfeller, Rocky Research Company, 1453 Rawhide Road, Boulder City, NV 89005
61. D. S. Severson, Gas Research Institute, 8800 West Bryn Mawr Avenue, Chicago, IL 60631
62. Sam. V. Shelton, Georgia Institute of Technology, Department of Mechanical Engineering, Atlanta, GA 30332
63. J. J. Tuzson, Gas Research Institute, 8800 West Bryn Mawr Avenue, Chicago, IL 60631
64. G. C. Vliet, Taylor Hall 116, The University of Texas, Austin, TX 78712
65. M. Wahlig, Lawrence Berkeley Laboratory, University of California, Berkeley, CA 94720
- 66-80. Energy Conservation Distribution, Oak Ridge National Laboratory, Building 9102-2, Room 103, Oak Ridge, TN 37831
81. Office of the Assistant Manager for Energy R&D, U.S. Department of Energy, Oak Ridge Operations, Oak Ridge, TN 37831
- 82-111. Technical Information Center, U.S. Department of Energy, P.O. Box 62, Oak Ridge, TN 37831